AGU PUBLICATIONS

JGR

Journal of Geophysical Research: Space Physics

RESEARCH ARTICLE
10.1002/2017JA024029

Special Section:
Observations, Simulations, and Theory of Electric Currents in the Solar System

An explanation of auroral intensification during the substorm expansion phase

Zhonghua Yao[1,2], I. J. Rae[1], A. T. Y. Lui[3], K. R. Murphy[4], C. J. Owen[1], Z. Y. Pu[5], C. Forsyth[1], D. Grodent[2], Q.-G. Zong[5], A. M. Du[6], and N. M. E. Kalmoni[1]

[1]Mullard Space Science Laboratory, University College London, Dorking, UK, [2]Laboratoire de Physique Atmosphérique et Planétaire, STAR Institute, Université de Liège, Liège, Belgium, [3]The Johns Hopkins University Applied Physics Laboratory, Laurel, Maryland, USA, [4]NASA Goddard Space Flight Centre, Greenbelt, Maryland, USA, [5]School of Earth and Space Sciences, Peking University, Beijing, China, [6]Institute of Geology and Geophysics, Chinese Academy of Sciences, Beijing, China

Abstract A multiple auroral onset substorm on 28 March 2010 provides an opportunity to understand the physical mechanism in generating auroral intensifications during a substorm expansion phase. Conjugate observations of magnetic fields and plasma from the Time History of Events and Macroscale Interactions during Substorms (THEMIS) spacecraft, of field-aligned currents (FACs) from the Active Magnetosphere and Planetary Electrodynamics Response Experiment (AMPERE) satellites, and from ground-based magnetometers and aurora are all available. The comprehensive measurements allow us to further our understanding of the complicated causalities among dipolarization, FAC generation, particle acceleration, and auroral intensification. During the substorm expansion phase, the plasma sheet expanded and was perturbed leading to the generation of a slow mode wave, which modulated electron flux in the outer plasma sheet. During this current sheet expansion, field-aligned currents formed, and geomagnetic perturbations were simultaneously detected by ground-based instruments. However, a magnetic dipolarization did not occur until about 3 min later in the outer plasma sheet observed by THEMIS-A spacecraft (THA). We believe that this dipolarization led to an efficient Fermi acceleration to electrons and consequently the cause of a significant auroral intensification during the expansion phase as observed by the All-Sky Imagers (ASIs). This Fermi acceleration mechanism operating efficiently in the outer plasma sheet during the expansion phase could be a common explanation of the poleward auroral development after substorm onset. These results also show a good agreement between the upward FAC derived from AMPERE measurements and the auroral brightening observed by the ASIs.

Key Points:
- We present simultaneous measurements of field-aligned currents from magnetosphere, ionosphere, and ground station for a substorm event
- Fermi acceleration related to the shrinkage of magnetic field in outer plasma sheet could lead to poleward auroral intensification
- Slow mode wave is generated during near-Earth current sheet expansion

Correspondence to:
Z. Yao,
z.yao@ucl.ac.uk

Citation:
Yao, Z., et al. (2017), An explanation of auroral intensification during the substorm expansion phase, *J. Geophys. Res. Space Physics*, *122*, 8560–8576, doi:10.1002/2017JA024029.

Received 13 FEB 2017
Accepted 8 AUG 2017
Accepted article online 14 AUG 2017
Published online 29 AUG 2017

1. Introduction

A magnetospheric substorm is a major space weather phenomenon, which includes significant disturbances in the magnetosphere, ionosphere, and upper atmosphere. A magnetospheric substorm typically consists of three phases: the growth phase, expansion phase, and recovery phase [*Akasofu*, 1964; *McPherron et al.*, 1973]. The Dungey cycle describes the circulation of magnetic and plasma energy in the magnetosphere [*Dungey*, 1961]. A Dungey cycle includes two reconnection sites, i.e., subsolar magnetopause reconnection and near-Earth magnetotail reconnection. Subsolar magnetopause reconnection inputs solar wind energy into the magnetosphere, while magnetotail reconnection releases energy from the magnetosphere to interplanetary space and toward the inner magnetosphere. If the dayside and nighside reconnection rates are equal, the magnetosphere can reach a state of steady magnetospheric convection. If the dayside input energy is greater than the nightside released energy (usually due to southward turning of the interplanetary magnetic field), magnetic and plasma energies would be accumulated in the tail lobe and plasma sheet, forming a substorm growth phase, characterized by the enhancement of the cross-tail neutral sheet current, as well as thinning of the plasma sheet [*Akasofu*, 1972; *Hones*, 1977; *Rostoker et al.*, 1980; *Baker et al.*, 1985].

Energy accumulation during a substorm growth phase is followed by a sudden energy release, which is named the substorm expansion phase. During the substorm expansion phase, the near-Earth magnetotail is highly dynamic, with the magnetic field becoming strongly perturbed [*Lui*, 1996] and the cross-tail currents being diverted into the ionosphere from the magnetosphere [*Boström*, 1964]. During the expansion phase, energy is

explosively released in the near-Earth region and energetic particles are injected into regions around geostationary orbit [*Liou et al.*, 2001]. The enhancement of Region 1 FACs is a typical feature for substorm expansion, which is also well known as the substorm current wedge (SCW) [*McPherron et al.*, 1973].

During a substorm, thin auroral arcs (mostly east-west aligned and narrowed in north-south direction) in the most equatorward region of the auroral oval are usually formed in the late growth phase, which is followed by an explosive poleward expansion [*Akasofu*, 1964; *Craven and Frank*, 1987]. The poleward auroral expansions often present wave-like features, which are suggested to be associated with plasma instabilities [*Liang et al.*, 2008; *Rae et al.*, 2009]. Multiple mechanisms are found in generating aurora during a substorm recovery phase and thus produce double auroral oval distribution consisting of a poleward region of discrete oval and a more diffuse equatorward oval [*Elphinstone et al.*, 1995; *Mende et al.*, 2002]. The trigger mechanisms for the substorm expansion onset remain very controversial [e.g., *Angelopoulos et al.*, 2008 and *Lui*, 2009]. Flow braking in the near-Earth magnetotail and near-Earth instabilities are two of the most prevalent explanations [*Shiokawa et al.*, 1997; *Pu et al.*, 1997; *Birn et al.*, 1999; *Nakamura et al.*, 2001; *Kepko et al.*, 2001; *Ohtani et al.*, 2002; *Cao et al.*, 2010; *Kalmoni et al.*, 2015]. Moreover, *Hsu and McPherron* [2003] indicate that approximately 60% of all substorms appear to be triggered by a number of events including interplanetary magnetic field transitions, a reduction in B_y or a sudden change in the solar wind dynamic pressure, and the remaining 40% are nontriggered events. Their results imply that substorm expansions may be triggered by multiple mechanisms. This controversy is the result of limited observations and the superposition of various processes occurring in the magnetotail at substorm onset, such that conclusively determining how substorm onset occurs is extremely difficult. However, during a pseudobreakup, the number of physical processes developing at substorm onset is limited, providing an excellent opportunity to study specific driving mechanisms [*Pulkkinen et al.*, 1998; *Rostoker*, 1998; *Partamies et al.*, 2003; *Yao et al.*, 2014]. The pseudobreakup usually describes an event with substorm-like activities (e.g., auroral intensification, field-aligned current formation, and magnetic dipolarization), however, with much smaller amplitudes and much shorter duration (e.g., a few minutes). A pseudobreakup is often observed during the late substorm growth phase and thus may lead to misidentification of a substorm onset [*Pu et al.*, 2010]. Similar to the pseudobreakup, auroral intensifications during the expansion phase may also be associated with relatively limited perturbation in the magnetic field and plasmas since these are not directly related to any major energy release process and thus are ideal to investigate fundamental processes related to substorm dynamics.

It has been shown that a substorm may have multiple onsets [*Murphy et al.*, 2014]. This has been established from the ground geomagnetic field perturbations observed from the ground [*Pytte et al.*, 1976], auroral intensifications [*Keiling et al.*, 2008; *Pu et al.*, 2010], global magnetic field dipolarizations in the near-Earth magnetotail [*Duan et al.*, 2011; *Palin et al.*, 2015], and substorm injections into geosynchronous orbit [*Nagai et al.*, 1983]. Previous studies also suggest that multiple auroral intensifications are related to multiple bursty bulk flows [*Nishimura et al.*, 2012]. However, it has been shown that a single flow burst can only contribute <10% of the energy (or current) needed for the SCW [*Yao et al.*, 2015; *Lui*, 2015]. Auroral intensifications after substorm onset are usually observed poleward of the substorm onset auroral arc [*Saito et al.*, 2010; *Tang et al.*, 2013], which is cited as evidence for the inside-out substorm model [*Lui*, 1996, 2004; *Henderson*, 2009]. Together with the outside-in model [*Baker et al.*, 1996], this is one of the two most popular substorm models [*Ohtani*, 2004]. Since multiple onset is a common feature of a substorm, the mechanism for auroral intensification during expansion phase is thus highly relevant in understanding substorm mechanisms.

The energy of the main electron population associated with auroral brightening is usually in the several keV range [*Albert*, 1967], slightly higher than the energy of the main population in the magnetotail [*Walsh et al.*, 2011]. A mechanism for parallel acceleration is thus required during the precipitation of magnetospheric electrons into the upper atmosphere to generate aurora. An auroral acceleration region with parallel electric potential drop is often believed to play an important role in the parallel acceleration of electrons at 1 to 2 R_E altitude [*Marklund et al.*, 2011]. Another acceleration process driven by wave-associated parallel electric fields is often called "Alfvénic acceleration" [*Hasegawa*, 1976; *Chaston et al.*, 2010]. In addition to the potential drop acceleration and Alfvénic acceleration, Fermi acceleration is also an important mechanism that can drive parallel electron acceleration. Although Fermi acceleration is not very often discussed in driving auroral intensification, it could be important in driving auroral brightening [*Sharber and Heikkila*, 1972], as it is often a result of the magnetotail dynamics [*Wu et al.*, 2006]. It is still an open question on how the intense aurora is generated during substorms.

In this paper, we present a substorm event on 28 March 2010 with four near-identical auroral intensifications. For the second, third, and fourth intensifications, the magnetic footprints of the Time History of Events and Macroscale Interactions during Substorms (THEMIS)-A, THEMIS-D, and THEMIS-E spacecraft (THA, THD, and THE) were located near the auroral breakup region, and each spacecraft detected magnetic field and plasma perturbations. Moreover, the Active Magnetosphere and Planetary Electrodynamics Response Experiment (AMPERE) satellites were conjugate to the auroral intensification region. Taken together with THEMIS spacecraft, ground-based magnetometers, and all-sky imagers, this provides a complete picture of both the magnetosphere and ionosphere during these auroral intensifications. This paper focuses on the mechanism operating during the second and third intensifications. The coordinated FACs in the magnetotail and ionosphere are analyzed, as well as the electron acceleration process that directly causes the auroral intensifications.

2. Observations

In this section, we detail the analysis with the coordinated measurements from the ground auroral imagers, ground magnetometers, and the AMPERE and THEMIS spacecraft during 06:20 UT to 06:50 UT on 28 March 2010. The THEMIS mission consists of three spacecraft in the inner magnetosphere at $X \sim -10\,R_E$ during the mission's magentotail seasons [*Angelopoulos*, 2009]. In this study, we use plasma measurements from the electrostatic analyzer (ESA) [*McFadden et al.*, 2008] and the solid-state telescope (SST) [*Angelopoulos et al.*, 2009] and magnetic field measurements from the fluxgate magnetometer (FGM) [*Auster et al.*, 2009]. At 06:30 UT, THEMIS-A, THEMIS-D, and THEMIS-E were located at $[-11.28, -1.96, -0.15]\,R_E$, $[-11.29, -2.07, 0.40]\,R_E$, and $[-11.24, -1.92, 0.32]\,R_E$, respectively, in geocentric solar magnetospheric (GSM) coordinates. THA and THE satellites were mainly separated in the Z direction by a distance of $0.47\,R_E$. Since the THD and THE satellites were located in close proximity and have similar magnetic field and plasma observations, we only present observations from THA and THE. Ground auroral cameras, ground magnetometers, and the AMPERE spacecraft provide a cross validation of the field-aligned currents and particle acceleration concluded from the in situ THEMIS measurements.

2.1. Conjugate Observations From All-Sky Imagers, Ground-Based Magnetometers, and the AMPERE Mission

Figure 1 shows the auroral observations from ASIs [*Mende et al.*, 2009]. The ASIs provide 256×256 pixel images, with a temporal cadence of 3 s. Figure 1 shows combined auroral imagers from the Gillam (GILL), Sanikiluaq (SNKQ), and Rankin Inlet (RANK) stations. Four intensifications are identified at 06:24:33 UT, 06:33:30 UT, 06:37:45 UT, and 06:48:15 UT. Figures 1a–1d present the first clear auroral images occurring within 1 min of each auroral intensification. It is clear that the auroral intensification develops increasingly poleward successively from Figures 1a to 1d. The footprints of THA and THE (indicated by the filled circles in each panel) are derived using the T04s model [*Tsyganenko and Sitnov*, 2005], which claims to reconstruct the global magnetic field during substorm periods. As shown in Figures 1a and 1b, the footprints of THEMIS spacecraft were poleward of the auroral breakup region for the first two auroral intensifications and were close to the third and fourth auroral intensification regions.

The poleward development of auroral intensification is consistent with the magnetic perturbations observed from ground-based stations collocated with ASIs (Figure 2). As can be seen from Figure 1, RANK is at a higher latitude than the other two stations. Following the four auroral intensifications in Figure 1, four distinct negative bays of the H component of the magnetic field are identified at ~06:23:30 UT, ~06:33:30 UT, ~06:37:45 UT, and ~06:47:30 UT based on data from these three stations, which represent the formation of a westward electrojet [e.g., *Rostoker et al.*, 1980]. The first significant negative bay was detected only at GILL station, corresponding to the first localized auroral intensification over GILL ASI station (Figure 1a). The second negative bay was detected by both GILL and SNKQ, corresponding to the second auroral intensification that was recorded at both GILL and SNKQ ASIs (Figure 1b). The third magnetic negative bay was detected by GILL, corresponding to the third auroral intensification that was mostly limited in the field of view at GILL ASI (Figure 1c). The fourth negative bay was detected by RANK, corresponding to the fourth auroral intensification detected by both RANK and GILL (Figure 1d). The four negative bays are very closely related to the four auroral intensifications, based on timing and locations. Although the geomagnetic negative bay cannot show the same clear poleward development as the ASIs due to their low spatial resolution, it is very clear that the fourth negative bay was at a higher latitude than the other three negative bays. Considering that the four auroral

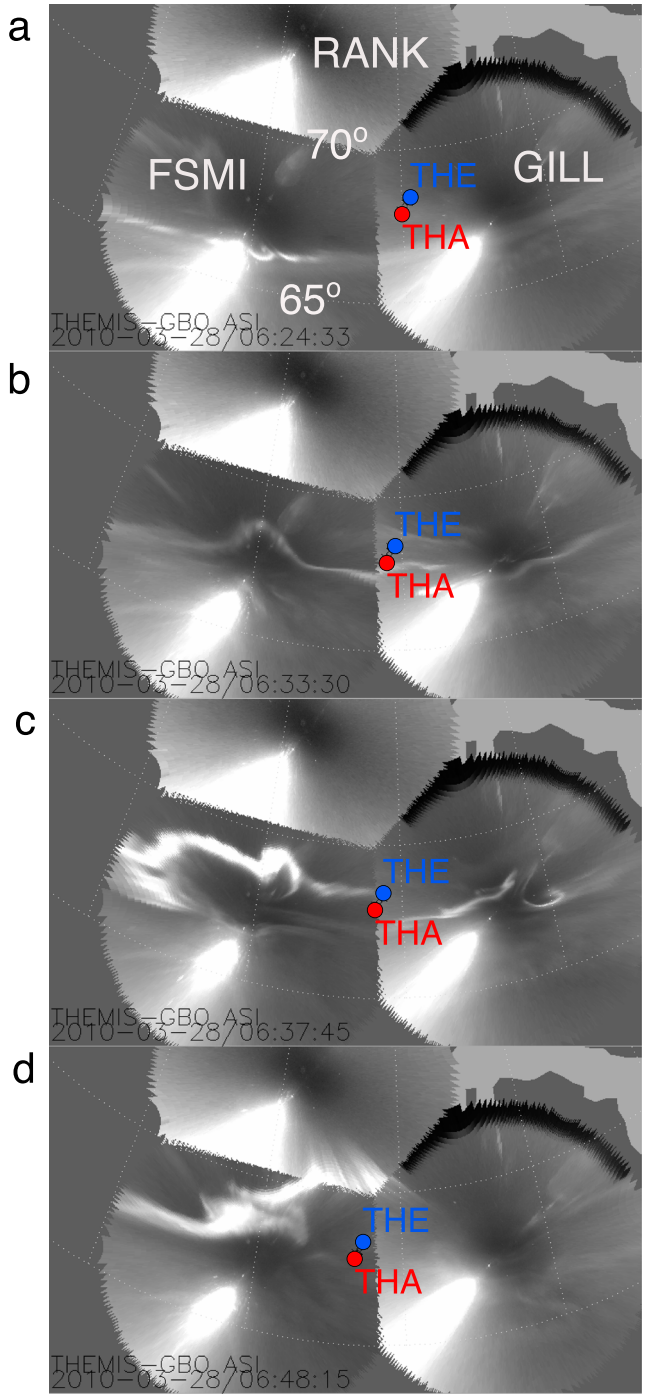

Figure 1. Auroral sequences from the North American THEMIS All-Sky Imagers (ASIs) at GILL, SNKQ, and RANK on 28 March 2010. The white dashed lines are invariant geomagnetic latitude and longitude. The two horizontal lines are separated by 5°, and the vertical lines are separated by 15°. The footprints of THA and THE are mapped based on the T04s model.

intensifications are very localized, and the associated current systems are likely localized as well, it is thus reasonable to detect the very different geomagnetic perturbations at these nearby stations. Specifically, the perturbations at SNKQ are generally much smaller than those at GILL, which is consistent with the auroral activities. For example, the third auroral intensification was mostly recorded by GILL at ~06:37:30 UT; meanwhile, a significant negative bay was observed by GILL, while only very slight perturbation was detected

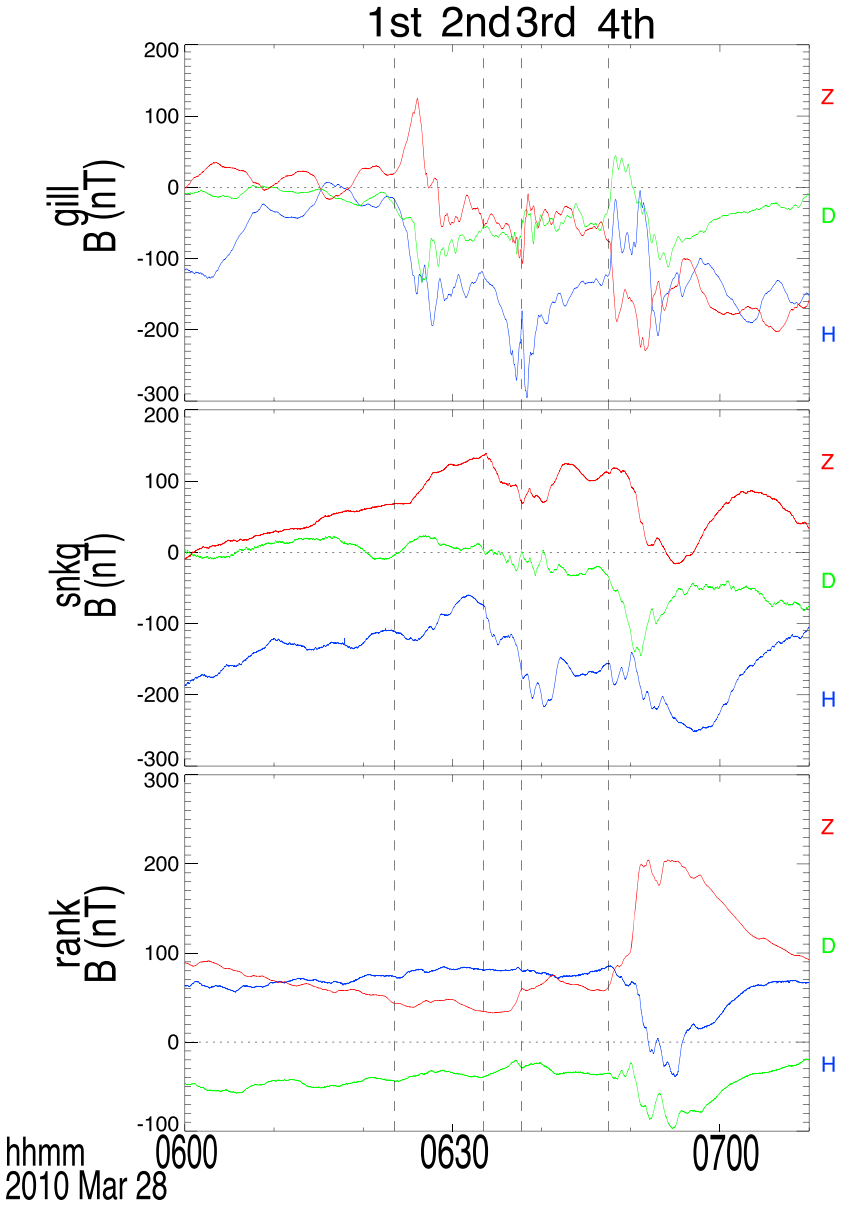

Figure 2. The component geomagnetic fields in a compass-type coordinate system (HDZ) from GILL, SNKQ, and RANK stations, which are in the same locations as the ASIs in Figure 1. The *H* component is the horizontal field strength, the *D* component is the declination component, and the *Z* component is the vertical component. The four vertical lines indicate four negative bays at 06:23:30 UT (GILL station), 06:33:30 UT (GILL and SNKQ), 06:37:45 UT (GILL), and 06:47:30 UT (RANK).

by SNKQ. At 2–3 min after the fourth negative bay recorded by RANK, SNKQ also detected a slight decrease, which is likely a consequence of the development of the localized auroral structure.

Figure 3 presents the global FAC distribution derived from AMPERE using vector magnetic field measurements from the Iridium constellation of low-Earth orbiting satellites [*Anderson et al.*, 2000; *Waters et al.*, 2001; *Murphy et al.*, 2012]. The global FAC distribution estimated from AMPERE is based on a quasi-stationary assumption on the timescale of spacecraft separation in each orbital track, i.e., ~10 min. Figure 3 presents the distribution of current density for 10 min periods from 06:16 UT to 06:56 UT. The data points with current density <0.2 $\mu A/m^2$ are discarded in Figure 3 to filter out noise. The green dots in Figure 3 represent the location of the GILL auroral imager/geomagnetic station. An upward FAC collocated at GILL station was significantly enhanced during the period represented in Figures 3b and 3c, and the footprints of THEMIS spacecraft were also mapped to the upward FAC region.

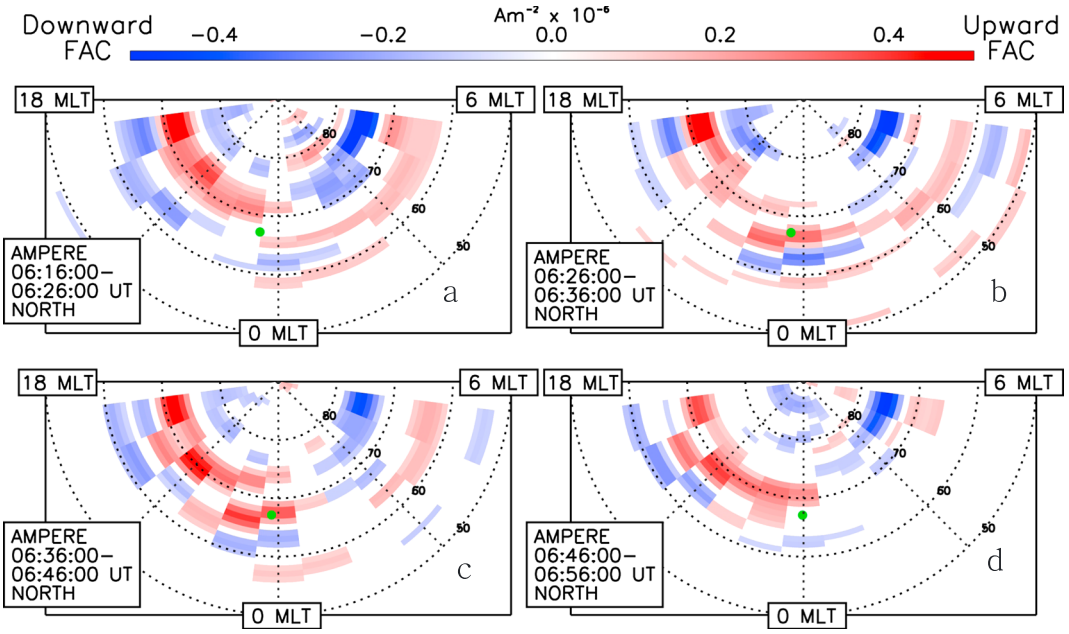

Figure 3. The field-aligned current distribution derived from AMPERE for the four time intervals as indicated in each plot. The green dot represents the location of GILL station.

The 10 min quasi-stationary assumption is typically not sufficient for substorm studies given that a substorm current wedge usually significantly develops within a few to tens of minutes [*Lui*, 1996; *Keiling et al.*, 2009; *Yao et al.*, 2012]. Therefore, it is not possible to fully determine whether the 10 min resolution upward FAC shown in Figure 3 is closely related to an auroral intensification since the auroral intensification developed within 1–2 min. To carefully interpret the AMPERE results, Figure 4a presents the 1 min resolution magnetic perturbations along the spacecraft's trajectory that cross the GILL station (<2° from the center), which provides a strong support to the explanation of FAC in Figure 3. The arrows in Figure 4a show AMPERE geomagnetic north-south and east-west magnetic field perturbations at 1 min resolution from the premidnight orbital track (23.1 magnetic local time (MLT)), which also travels through the GILL station. The FAC in Figure 3 is exactly

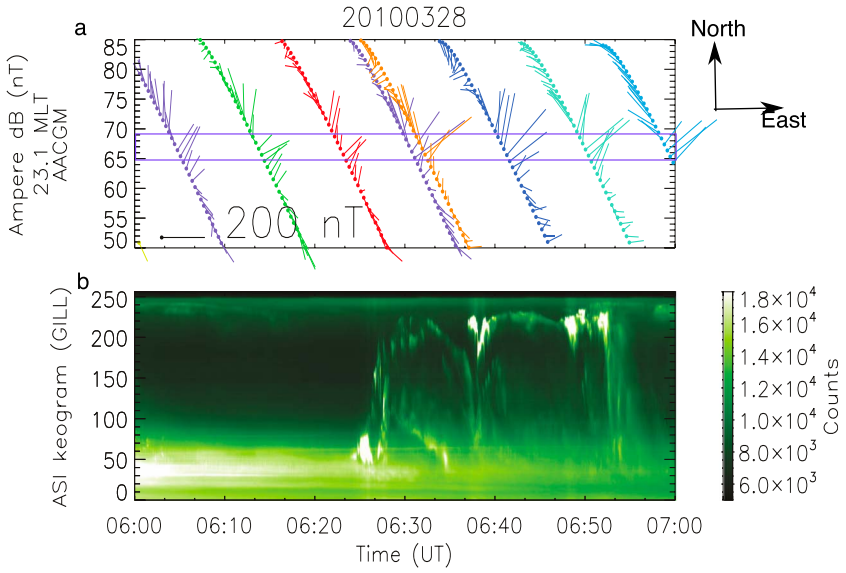

Figure 4. (a) The 1 min resolution magnetic perturbations along the premidnight orbital trajectory (23.1 MLT) that also cross the GILL station. The purple rectangle indicates the field of view of GILL station. Different colors represent the measurements from different spacecraft along the same orbital trajectory. (b) The keogram auroral image of GILL ASI station.

derived from the magnetic perturbations in Figure 4a (include all orbital tracks) based on Ampere's law. The coverage of a single ASI is approximately circular in geographic coordinates (radius of about 4.5°). The purple rectangle in Figure 4a indicates field of view of the GILL station. The trace of AMPERE spacecraft within the rectangle suggests conjugate measurements between AMPERE and GILL (the same MLT and the same latitude at the same time). Figure 4b shows the keogram of auroral images from the GILL station. These results indicate that the magnetic perturbations related to second, third, and fourth auroral intensifications were recorded by AMPERE spacecraft soon after these intensifications.

2.2. Overview of the In Situ Observations From THEMIS Spacecraft

Figure 5 shows the magnetic field and plasma measurements for this event from THA and THE satellites. Figures 5a and 5b give the magnetic field components and magnetic field strength at a 3 s resolution in GSM coordinates. Figures 5c and 5d present the perpendicular components of the ion bulk velocity. The magnetic field was >35 nT before ~06:33 UT at both spacecraft, and dominated by B_x, suggesting that the two spacecraft were away from the central plasma sheet. Figure 5e shows plasma pressure for both spacecraft. As given by Figure 5f, the plasma beta (ratio between plasma pressure and magnetic pressure) was between 0.1 and 1, which indicates that both spacecraft were located in the outer plasma sheet [e.g., *Baumjohann et al.*, 1989]. After 06:33 UT, until ~06:40 UT, the magnetic field B_x component at THA started to decrease, accompanied by clear oscillations, while the magnetic field at THE is not obviously perturbed between ~06:33 UT and ~06:40 UT. B_x at THE slightly decreased after ~06:36:30 UT. At ~06:48 UT, intense perturbations were detected by THA and THE, which corresponds to the fourth auroral intensification. The present paper focuses on the measurements between 06:30 UT and 06:40 UT. Overall, the plasma pressure is anticorrelated with magnetic field strength for both spacecraft. Particularly for THA, the wave-like plasma pressure variation is highly anticorrelated with the magnetic field strength. The details of these oscillations are presented in section 2.3.

Figure 5g shows the current density estimated from the magnetic field measured by THA and THE satellites. The current density J_x and J_y in GSM coordinates were derived from Ampere's law by assuming that the measured magnetic field consists of two components, i.e., quasi-steady dipole field and a 1-D current sheet [e.g., *Lui*, 2011, 2013; *Yao et al.*, 2014]. In the estimation of current density, it is assumed that $\frac{\partial}{\partial z} > \frac{\partial}{\partial x}, \frac{\partial}{\partial y}$. The current density is thus simply given by $J_x \sim \frac{\partial B_y}{\partial z}$ and $J_y \sim -\frac{\partial B_x}{\partial z}$. We would like to point out that the assumptions applied in the current density calculation may only be valid when both spacecraft were located in the outer plasma sheet, where B_x is the dominant magnetic field. In the central plasma sheet, the $\frac{\partial}{\partial x}$ term may be more significant than the $\frac{\partial}{\partial z}$ term. On the other side, the current density embedded between THA and THE with MHD theory (diamagnetic current) can be derived as an independent calculation from the Ampere's law [e.g., *Yao et al.*, 2014, equation 4]. Figure 5g shows the diamagnetic current density J_y (from MHD theory) with the averaged pressure gradient ($\nabla_z P$) and averaged magnetic field (B_x) between THA and THE. It is clear that the variation of the diamagnetic current density is very consistent with, however, obviously smaller than the magnetic derived current density. This might be a consequence of a nonuniform current density distribution of the current sheet. The current density J_y started to increase (up to ~6 nA/m^2) after ~06:33 UT, which is consistent with the magnetic field B_x decrease and plasma pressure increase at THA. The increase of current density could be due to current sheet expansion or current sheet moving toward the spacecraft. However, from the measurements at THE, the spacecraft was not moving closer to the central plasma sheet, since the magnetic field was stable, and plasma pressure (also beta value) showed a decrease after 06:33 UT rather than the increase as expected if the center of the current sheet was moving closer to the spacecraft. It can thus be concluded that this localized cross-tail current density enhancement is due to current sheet expansion, which does not imply an enhancement of the total cross-tail current. The current sheet expansion is also consistent with the auroral intensification at ~06:33:30 UT as shown in Figure 1b. After 06:37:00 UT, the current density J_x is enhanced up to ~3 nA/m^2. Since the magnetic field is still dominated by B_x, J_x thus can roughly represent the field-aligned current. This enhancement of J_x is likely to be related to the timing of the third auroral intensification at ~06:37:45 UT shown in Figure 1c.

2.3. Slow Mode Wave in the Magnetotail: THA Observations

It was shown that the wave-like perturbations were observed in the magnetic field and plasma pressure for the THA satellite between ~06:33 UT and ~06:40 UT. This section presents the detailed characteristics of these perturbations in the measurements of THA satellite. Figure 6a presents the magnetic field in the mean field coordinate system, which is determined using low-pass-filtered data with a shortest period of 600 s. The mean

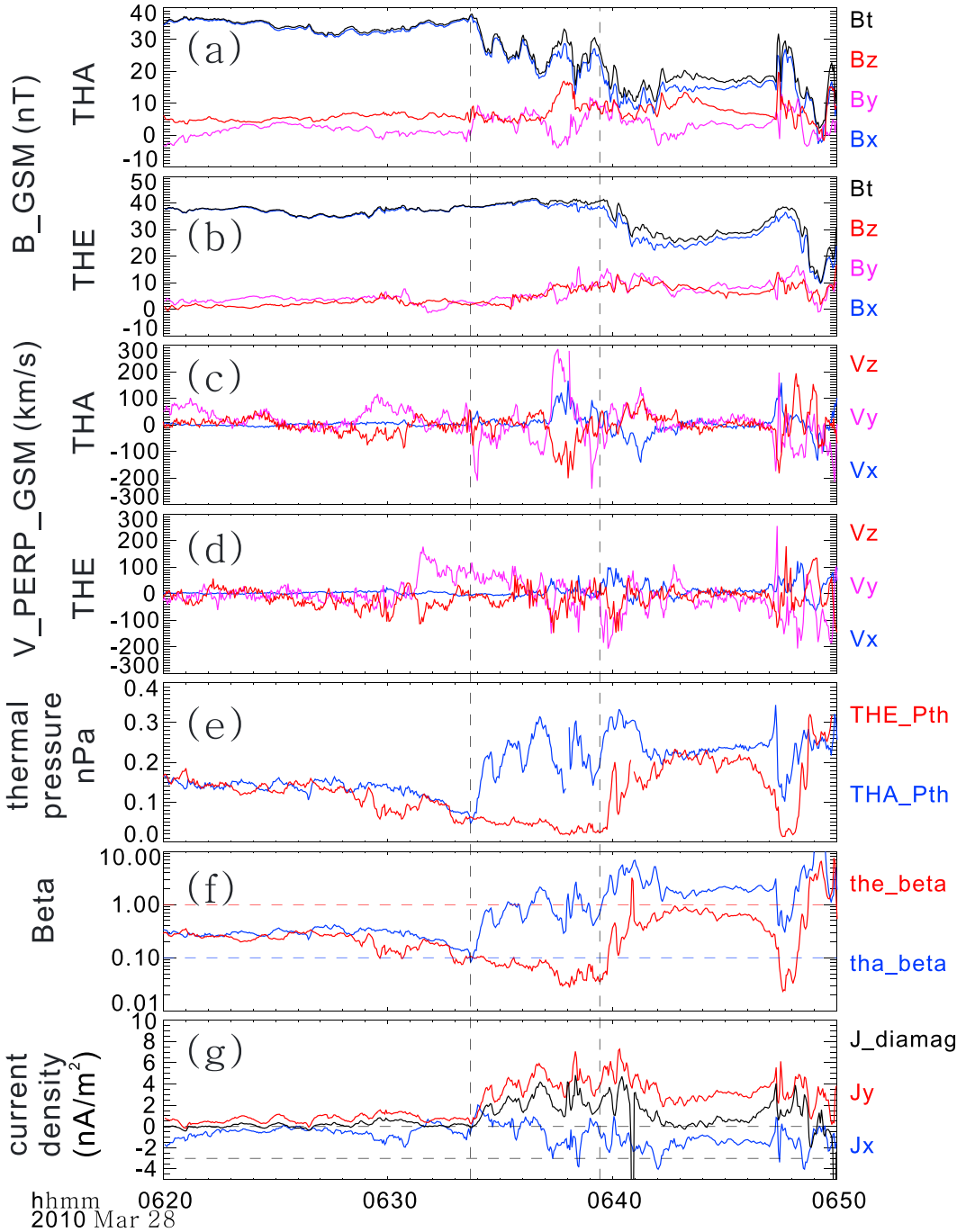

Figure 5. Overview of THA and THE observations. (a and b) The magnetic components in GSM coordinates and the total magnetic strength. (c and d) The ion bulk velocity in GSM coordinates. (e and f) The plasma pressure and beta value of THA and THE. (g) The current density derived from Ampere's law and the diamagnetic current (the black line). The two dashed vertical lines indicate the start of B_x decrease at THA and THE, implying a step-like current sheet expansion.

field coordinate is defined as follows: the direction **b** is along the mean magnetic field, **a** points eastward, and **r** completes the right orthogonal set. Figure 6b shows band-pass-filtered results of the magnetic field in the mean field coordinate system. Figures 6c and 6d show the detrended band-pass-filtered plasma and magnetic pressure variations. Figures 6b–6d have adopted 40 s to 120 s as the band-pass filter, which contains the period of the main magnetic and plasma pressure perturbations that could be clearly identified by eye from Figure 5.

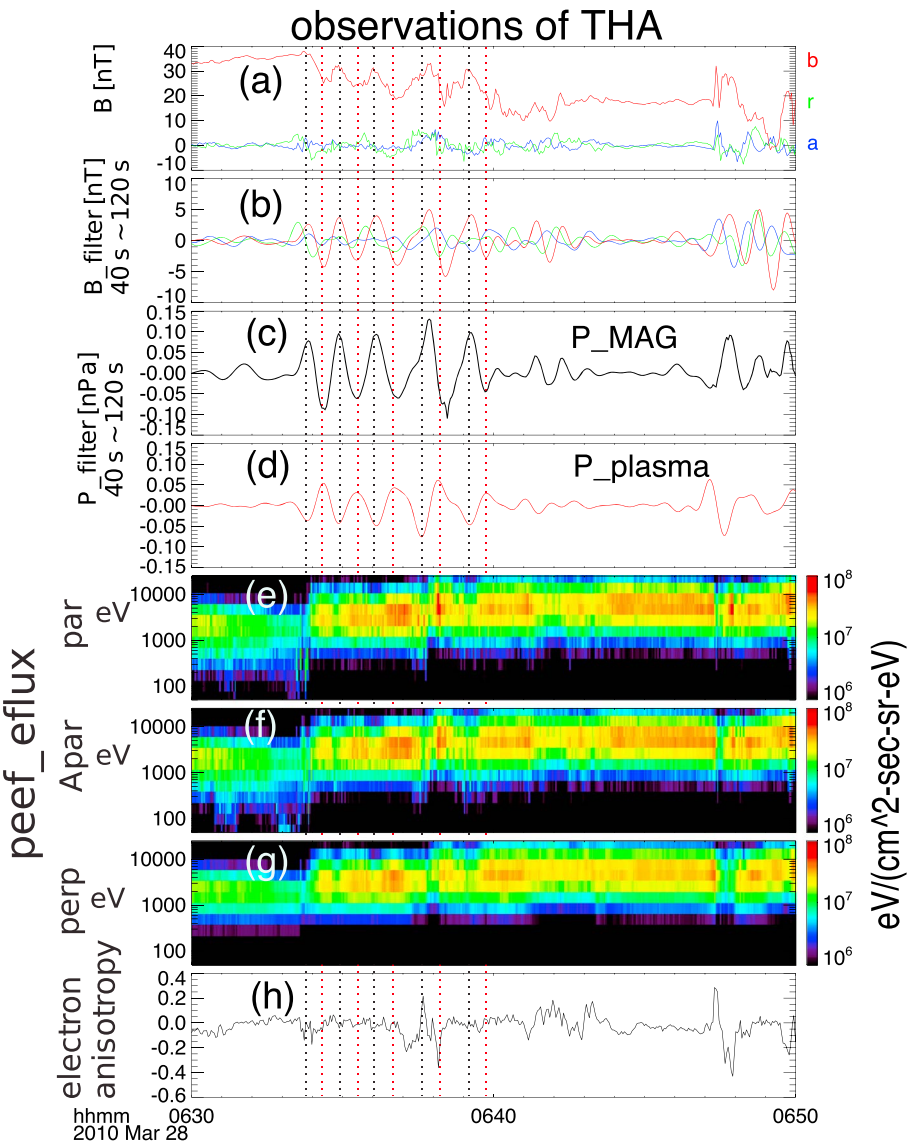

Figure 6. Observations of THA. (a) The magnetic field in mean field coordinate. (b) The filtered magnetic field with band-pass filter between 40 s and 120 s. (c and d) The filtered magnetic and plasma pressure with band-pass filter between 40 s and 120 s. (e–g) The electron differential energy flux for parallel, antiparallel, and perpendicular pitch angle populations. (h) The electron anisotropy index, which is defined by $T_{perp}/T_{par}-1$. The dashed vertical lines indicate the magnetic pressure peaks (plasma pressure troughs, black) and the magnetic pressure troughs (plasma pressure peaks, red).

The perturbations of plasma pressure and magnetic strength observed by THA satellite could be related to plasma sheet flapping [*Sergeev et al.*, 2003; *Runov et al.*, 2005; *Nakamura et al.*, 2006] or compressional waves [*Volwerk et al.*, 2003; *Du et al.*, 2011]. As shown in *Forsyth et al.* [2009], during plasma sheet flapping, two magnetic field components $|B_x|$ and B_z in GSM coordinates should be anticorrelated. In this event, $|B_x|$ and B_z are correlated, which suggests that the perturbations are likely to be a compressional wave. Since magnetic strength is out of phase with plasma pressure variation, and the magnitudes of plasma and magnetic perturbation are comparable (i.e., ~0.05–0.1 nPa), it can thus be concluded that this is a slow mode wave [*Nakamizo and Iijima*, 2003]. As shown in Figure 6b, the transverse components of the magnetic fluctuations are smaller than the compressional component. This indicates that the slow mode wave is the dominant perturbation, accompanied by small Alfvénic perturbations.

Figures 6e–6g show the spectrum of parallel (0° pitch angle (PA)), antiparallel (180° PA), and perpendicular (90° PA) differential energy flux of electrons. As indicated by the dashed vertical red lines, the electron

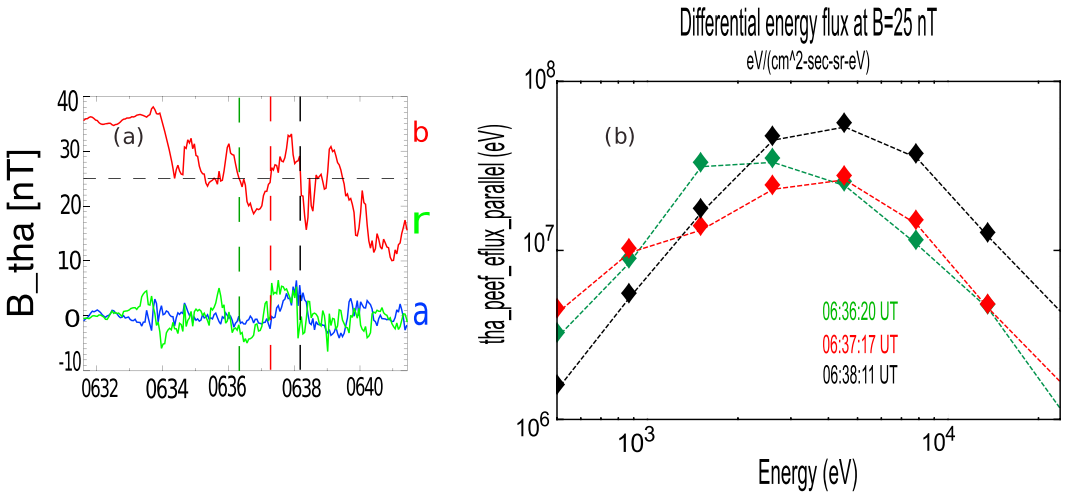

Figure 7. (a) The same plot as shown in Figure 6a. The three vertical lines indicate the time when B_b is 25 nT. (b) The parallel differential energy flux for the three given time intervals as indicated by the three vertical lines in Figure 7a.

differential energy flux is significantly enhanced at the magnetic troughs (plasma pressure peak), which is likely a consequence of modulation of the fluxes by the slow mode wave. Figure 6h shows an index of the electron anisotropy, which is defined as $T_{perp}/T_{par} - 1$. The $T_{par} > T_{perp}$ anisotropy feature became significant at ~06:36:47 UT, about 50 s before the third auroral intensification. An explanation for this electron anisotropy increase is presented in section 2.4.

The data plotted in Figure 7a are the same as Figure 6a. The dashed horizontal line in Figure 7a indicates the value of 25 nT, and the three vertical dashed lines indicate the three time points when B_b was 25 nT. The three time points were 06:36:20 UT, 06:37:17 UT, and 06:38:11 UT. To examine the electron acceleration features during the current sheet expansion, we compare the electron differential energy flux distribution for the three time snapshots indicated by the vertical dashed lines in Figure 7a. As discussed above, the electron flux is modulated by the slow mode wave; it is thus important to distinguish the acceleration effect from the modulation effect. The modulation effects (shown in Figures 6d–6f) at the three time points (the three vertical lines in Figure 7a) with the same B_b value can be considered to be similar, so the electron acceleration effects could be determined by comparing the flux distribution of parallel electron population as shown in Figure 7b. The distribution at 06:38:11 UT clearly shows a decrease at low energies (<1 keV) but an increase at high energies (>2 keV) compared to the two earlier distributions. This is a feature of electron acceleration [e.g., *Angelopoulos et al.*, 2008]. This significant field-aligned acceleration is consistent with the expectations of Fermi acceleration as explained in the next section.

2.4. Fermi Acceleration and Auroral Intensification

The physical process leading to the field-aligned acceleration of electrons shown in Figure 7b is discussed in this section. The magnetic field components from THA satellite are shown in Figure 8a (the same as Figure 5a). Figure 8b presents the averaged energy flux of parallel, perpendicular, and antiparallel electrons with energy between 2 keV and 5 keV. It is clear that the energy flux at all pitch angles is peaked at the magnetic troughs, which are indicated by the dashed vertical lines. However, after the magnetic trough at 06:36:45 UT (indicated by the solid vertical line), the field-aligned electron population did not immediately decrease, with the drop of perpendicular population as occurred in the two previous magnetic troughs. Instead, the parallel and antiparallel populations continued to increase for ~20 s as indicated by the black arrow in Figure 8b.

Figure 8c shows the magnetic field elevation angle at THA, which is defined as atan(B_z/B_x). The elevation angle significantly increases from ~10° before ~06:37 UT to up to 40° at ~06:38 UT. This elevation angle change occurs at ~3 min after the start of B_x decrease, which corresponds to the current sheet expansion. The variation of elevation angle suggests that the global magnetic reconfiguration (i.e., magnetic dipolariation), THA, thus moved relative to the central plasma sheet during this period. The magnetic dipolarization could be associated with a shrinking of magnetic field line, particularly for the field lines in the outer plasma sheet that are thought to be highly stretched prior to substorm onset. The shrinking of a magnetic field line causes

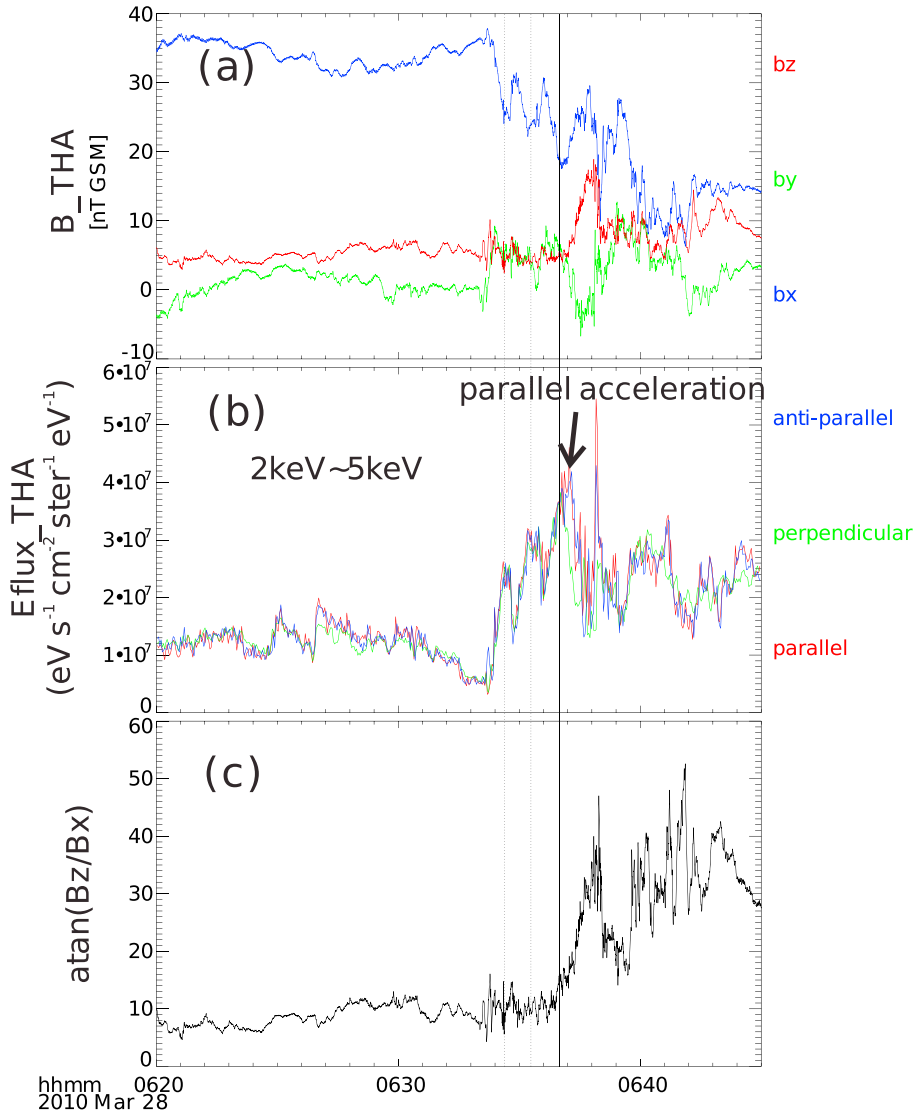

Figure 8. (a) The magnetic field of THA in GSM coordinates. (b) The averaged electron energy flux between 2 keV and 5 keV, for parallel, perpendicular, and antiparallel pitch angles. (c) The magnetic field elevation angle at THA, which is defined as atan(B_z/B_x). The vertical lines in Figures 8a–8c indicate magnetic troughs, which corresponds to the peaks of perpendicular fluxes, suggesting that the electron fluxes were modulated by the magnetic variation. For the first two dashed vertical lines, the parallel/antiparallel electron fluxes varied the same as the perpendicular, while after ~06:36:40 UT (indicated by the solid vertical line) the parallel/antiparallel continues to increase after the magnetic trough (indicated by the black arrow), suggesting a field-aligned acceleration.

efficient parallel acceleration, i.e., a first-order Fermi acceleration, which is energy dependent [e.g., *Parks*, 2008, equation 4.125]. We are not aware of any in situ observations of this energy dispersion effect associated with Fermi acceleration in previous literature, while the energy-dependent effect could be explained by a simple picture. For example, the bouncing period for field-aligned electrons with energy at 100 eV is 3 times longer than those with energy at 900 eV. If the 900 eV electrons take 10 s to finish a bounce, then the 100 eV electrons need 30 s to finish a bounce. So in this situation, the 900 eV electrons can be accelerated after 10 s, while the 100 eV electron would not be accelerated until 30 s after the magnetic shrink. Figure 9 presents the energy flux anisotropy, i.e., Eflux(PA: 0°) − Eflux(PA: 90°) versus energies. It is clear that the >5 keV populations were first enhanced, while lower energy populations were enhanced later. This energy dispersion is an important evidence for Fermi acceleration.

As a supplement to the energy dispersion shown in Figure 9, Figures 10a and 10b show the pitch angle distributions in energy in a spectrum format for two time intervals, i.e., 06:37:05 UT to 06:37:08 UT and 06:37:20 UT

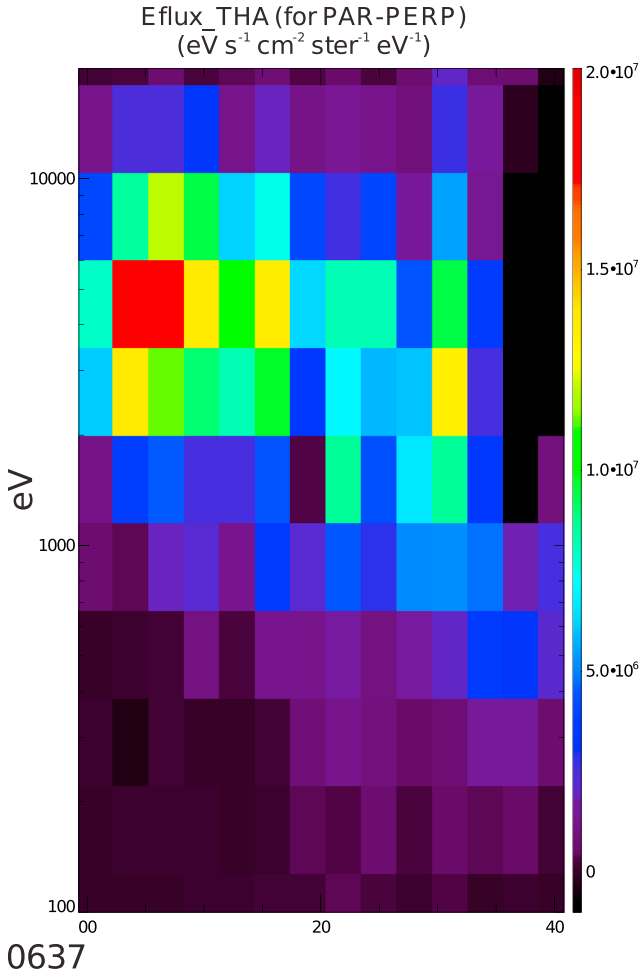

Figure 9. The energy dispersion associated with the parallel acceleration: Eflux(PA: 0°) − Eflux(PA: 90°) versus energies.

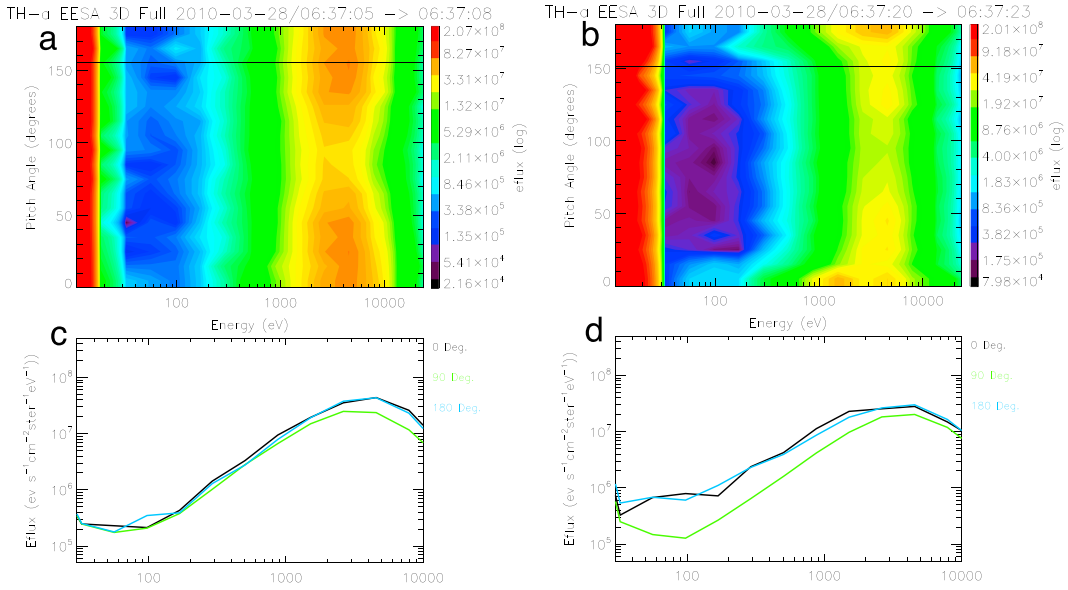

Figure 10. The electron pitch angle distribution of THA for two given time intervals. (a and b) The pitch angle distributions in energy in a spectrum format for two time intervals, i.e., 06:37:05 UT to 06:37:08 UT and 06:37:20 UT to 06:37:23 UT. (c and d) The electron fluxes along (0° PA), opposite (180° PA), and perpendicular (90° PA) to the magnetic field for the two time intervals.

to 06:37:23 UT. Figures 10c and 10d show the electron fluxes along (0° PA), opposite (180° PA), and perpendicular (90° PA) to the magnetic field for the two time intervals of Figures 10a and 10b. In the pitch angle distribution collected between 06:37:05 UT and 06:37:08 UT (Figures 10a and 10c), a clear bistreaming distribution appears at energy above 2 keV, and in the distribution measured between 06:37:20 UT and 06:37:23 UT (Figures 10b and 10d), a clear bistreaming distribution feature appears at much larger energy range, including energies between 100 eV and 2 keV. It is clear that this parallel acceleration is energy dependent and started from high energy.

3. Discussion and Summary

Conjugate measurements from THEMIS spacecraft, AMPERE satellite, geomagnetic stations, and all-sky imagers have been presented for a substorm event on 28 March 2010 with four near-identical auroral intensifications. The AMPERE observations also show a consistent upward FAC in the auroral brightening region soon after the second, third, and fourth intensifications. The auroral brightening shows a clear trend of poleward development, which is consistent with the geomagnetic measurements in the same region. The coordinated in situ observations of the magnetic field and plasma perturbations from the near-Earth THEMIS spacecraft have been presented for the second, third, and fourth intensifications. The corresponding magnetotail perturbation for the first intensification was not detected by THEMIS because the auroral breakup region was at a too low latitude, as indicated by the foot points from T04s model in Figure 1.

At ~06:33 UT, THA detected a B_x decrease and plasma pressure increase, which suggest an expansion of current sheet. The corresponding ionospheric electrojet feature and auroral intensification were also detected by GILL and SNKQ geomagnetic/auroral stations considering that the transit Alfvén time between the near-Earth magnetotail and ground is usually tens of seconds to 1 min [*Lui et al.*, 2010; *Sergeev et al.*, 2011; *Yao et al.*, 2013]. Although THA detected the decrease of B_x, the magnetic field did not dipolarize, as indicated by data shown in Figure 8c. This suggests that the current sheet expansion itself may not contribute significantly to any current diversion into the ionosphere at the distance of THA/THE probes. Instead, the ionosphere electrojet associated with GILL and SNKQ is likely to be inward of the spacecraft locations in the magnetotail. In this paper, it is very difficult to determine the exact mechanism for the current diversion as there was no spacecraft detecting the perturbation in the central plasma in the inner region. Near-Earth plasma instabilities and flow braking might be the potential mechanisms in driving the current diversion [*Pu et al.*, 1997; *Birn et al.*, 1999; *Ohtani et al.*, 2002]. The reason to suggest inner region rather than outer region is that the auroral intensification was observed at latitudes lower than those of the spacecraft's foot points. On the other hand, the magnetic field strength at THE that could roughly represent the lobe field strength was very stable after the current sheet expansion. This feature also suggests that the total cross-tail current (the current density integrated along the Z direction) at this distance was not significantly diverted into the ionosphere. The B_x component starts to decrease at ~06:36:30 UT, when the field-aligned currents also start to increase. The time delay between current sheet expansion and total cross-tail current reduction could be a common feature of many substorms, as a similar delay can be observed in another event reported by *Lui* [2011]. During the substorm expansion, the magnetotail current sheet expands and a portion of the cross-tail currents diverts into the ionosphere to form substorm current wedge. However, the cross-tail current diversion is usually initiated from a region in the near-Earth plasma sheet then spreads farther tailward [e.g., *Lui*, 1996]. It is thus very likely that at a given radial distance, the total line current density (current density integrated along Z direction) may not be reduced at substorm onset. On the other hand, during substorm onsets, the plasma pressure is significantly changed, which causes the redistribution of the cross-tail current density [*Yao et al.*, 2012; *Birn and Hesse*, 2013]. This current redistribution is very likely to enhance current density in certain regions, although the total global current should decrease. Combining the effects from the current diversion into the ionosphere and current redistribution in the magnetosphere, it is thus reasonable to expect to observe both the cross-tail current decreases and increases a few minutes after substorm onset. In *Lui* [2011], the total current density is irregular within ~8 min after substorm onset and is then followed by an eventual decrease.

During the current sheet expansion at ~06:33 UT, a slow mode wave was excited (section 2.3). As shown in Figure 6, the electron flux was significantly modulated by this slow mode wave. An AMPERE spacecraft also traveled across the auroral intensification region between ~06:30 UT and 06:33 UT (Figure 4) and detected large magnetic perturbations corresponding to an upward field-aligned current (Figure 3). *Du et al.* [2011] studied the mode conversion between slow mode wave and Alfvén wave; in their paper, they found

that the wave mode strongly relies on the direction of background magnetic field. They also show that an Alfvén wave excited in the neutral sheet region would be converted to a compressional wave when this wave propagates to higher latitude. This is also consistent with theoretical results of *Southwood and Saunders* [1985] that the coupling of slow mode and Alfvén wave can occur in the region in which the magnetic field line is sharply bent (e.g., the central current sheet in the highly stretched magnetotail). However, in the event reported here, the slow mode appears to have been excited in a less bent magnetic field configuration, where B_x is dominant. The slow mode wave is also considered as a physical nature of Pi2 pulsation in the magnetotail, which are suggested to be a key feature of substorm expansion [*Kepko et al.*, 2001; *Xing et al.*, 2015]. The slow mode wave and upward FAC are likely two independent consequences of current sheet expansion, although we could not determine the exact mechanism of current sheet expansion.

About 4 min after the current sheet expansion, a magnetic dipolarization was observed by THA, which would naturally be associated with the shrinking of the magnetic field line length. Meanwhile, field-aligned currents were also formed as shown in Figure 5g. Although the field-aligned currents were formed at the same time as Fermi acceleration, this does not imply that the Fermi acceleration generates the field-aligned current, although they might both be related by other fundamental dynamics. As was previously mentioned, the generation of field-aligned current is not investigated in this paper. The magnetic field line shrinkage causes Fermi acceleration, which leads to the third auroral intensification. Moreover, a clear energy dispersion feature for the parallel acceleration of electrons has been detected, which is strong evidence for Fermi acceleration. It is noteworthy that energy dispersion is a common feature of reconnection acceleration. However, the reconnection accelerated electron would likely show a time delay between the earthward and tailward populations, as the tailward electron beam is a reflection of an earthward electron beam at the ionospheric mirror point. Particularly, we would like to introduce the Cluster observations of X line accelerated electron beams in the near-Earth magnetotail by *Alexeev et al.* [2006]. The time delays for electrons with energies at hundreds eV to keV would be tens of seconds. From Figure 8, we do not find such a time delay between the enhanced parallel and antiparallel electron beams (at ~06:37 UT). From a zoom in plot of Figure 8 (not shown here), a time delay of ~3 s between the parallel and antiparallel populations can be identified, which is about a spacecraft spin period (i.e., the temporal resolution of plasma distribution function). This time delay is significantly shorter than a keV electron to complete a round-trip from the spacecraft location to the ionospheric mirror point (~7 s). Thus, it is most likely that the parallel/antiparallel electron acceleration was a consequence of Fermi acceleration, although it is difficult to fully rule out the possibility of reconnection acceleration in consideration of the complexity of magnetic reconnection (e.g., unsteady reconnection). Fermi acceleration occurring during the magnetic dipolarization in the outer plasma sheet, during expansion phase, could be an efficient form of acceleration during substorms, which may directly cause a most well-known feature of auroral substorms, i.e., auroral poleward expansion after substorm onset [*Lui et al.*, 2008; *Liang et al.*, 2008; *Rae et al.*, 2009; *Henderson*, 2009]. Although Fermi acceleration associated with magnetic dipolarization is often discussed [*Fu et al.*, 2011; *Birn et al.*, 2012, 2013], the energy dispersion associated with Fermi acceleration has not been reported in previous literature that we are aware of. Two potential reasons are suggested here: (1) to present the energy dispersion feature, a spacecraft must measure an ongoing acceleration; the acceleration would be efficient to electrons with energies at hundreds of eV to a few keV within tens of seconds, and the dispersion feature would thus disappear, and (2) in the magnetotail, a dipolarization is likely accompanied by many other dynamics that may lead to pitch angle scattering and particle acceleration. The mixture of multiple processes makes it difficult to identify the energy dispersion associated with Fermi acceleration. In previous studies, poleward auroral expansions are usually explained as the consequence of tailward propagation of cross-tail current disruption [*Lui*, 1991; *Jacquey et al.*, 1993]. The observations show that current sheet expansion does not necessarily simultaneously cause a dipolarization or current diversion into the ionosphere at a given distance (e.g., the spacecraft location in this event). Instead, the dipolarization could occur at a few minutes after current sheet expansion (or the ionosphere electrojet formation), which causes Fermi acceleration and the consequent auroral brightening after substorm onset. This work provides important information in understanding the relation between auroral brightening and FAC formation. Moreover, the field-aligned electron distribution observed in the near-Earth magnetotail is not an unusual feature during substorms [*Lui*, 2004], which is also suggested to be related to the nonlinear consequence of the physical process activated during current disruption. Considering that the magnetic field measured by the THEMIS spacecraft (~20 nT) is much smaller than the magnetic field in the conjugated ionosphere mirror point ($\sim 6 \times 10^4$ nT), the loss cone population (~1°) is too small to be resolved by the THEMIS electron instrument.

In the substorm event on 28 March 2010, coordinated observations between the magnetotail perturbations, the ionosphere FAC, the ground geomagnetic perturbations, and the ground aurora intensifications are detailed. The simultaneous measurements from instruments magnetically connected from magnetosphere to ionosphere and ground provide a good opportunity to study the magnetospheric mechanism for the poleward auroral intensification during substorm expansion phase. In conclusion, by analyzing the conjugate observations from in situ and ground measurements, the new findings in this paper are summarized as follows:

1. The energy dispersion associated with Fermi acceleration was detected during a substorm poleward auroral intensification when magnetic dipolarization was also detected in the near-Earth magnetotail.
2. Apart from the two prevalent mechanisms of auroral particle acceleration (the parallel electric potential drop in auroral acceleration region and the Alfvénic acceleration), Fermi acceleration can be another important but less discussed mechanism, since it occurs as a very natural consequence of magnetotail current redistribution and become particularly efficient in the outer plasma sheet region where the magnetic field is usually highly stretched.
3. The magnetic dipolarization in the outer plasma sheet occurred a few minutes after current sheet expansion, which resulted in a stepwise auroral development.
4. During the plasma sheet expansion, slow mode compressional wave was excited, which modulates the electron flux, but causes neither significant anisotropy nor acceleration.

Acknowledgments
We thank the AMPERE team and the AMPERE Science Center for providing the Iridium-derived data products. We acknowledge NASA contract NAS5-02099 and V. Angelopoulos for use of data from the THEMIS mission. Specifically, we thank J.W. Bonnell and F.S. Mozer for the use of EFI data; K.H. Glassmeier, U. Auster, C.W. Carlson, and J.P. McFadden for the use of ESA data; D. Larson and R. P. Lin for the use of SST data; and W. Baumjohann for the use of FGM data provided under the lead of the Technical University of Braunschweig and with financial support through the German Ministry for Economy and Technology and the German Center for Aviation and Space (DLR) under contract 50 OC 0302. The authors thank I.R. Mann, D.K. Milling, and the rest of the CARISMA team for data. CARISMA is operated by the University of Alberta, funded by the Canadian Space Agency. We also thank S. Mende and E. Donovan for the use of the ASI data, the CSA for logistical support in fielding and data retrieval from the GBO stations, and NSF for support of GIMNAST through grant AGS-1004736. Z.Y. thanks the useful discussion with Andrew Fazakerley at MSSL. Z.Y. is supported by UK Science and Technology Facilities Council (STFC) grant (ST/L005638/1) at UCL/MSSL. I.J.R. is supported by STFC grant (ST/L000563/1) and National Environmental Research Council (NERC) grant (NE/L007495/1), and C.F. is supported by NERC grant (NE/L007495/1). This work is also supported by NSFC grant (41525016 and 41404117). Z.Y. is a Marie Curie COFUND postdoctoral fellow at the University of Liege, cofunded by the European Union. We would like to acknowledge the QSAS science analysis software for space plasma data. The THEMIS data are available from http://themis.ssl.berkeley.edu/data/themis/.

References

Akasofu, S.-I. (1964), The development of the auroral substorm, *Planet. Space Sci.*, *12*(4), 273–282.
Akasofu, S.-I. (1972), Magnetospheric substorms: A model, in *Solar-Terrestrial Physics*, edited by E. R. Dyer and J. G. Roederer, pp. 531–551, Springer, Netherlands.
Albert, R. D. (1967), Nearly monoenergetic electron fluxes detected during a visible aurora, *Phys. Rev. Lett.*, *18*(10), 369–372.
Alexeev, I., V. Sergeev, C. Owen, A. Fazakerley, E. Lucek, and H. Reme (2006), Remote sensing of a magnetotail reconnection X-line using polar rain electrons, *Geophys. Res. Lett.*, *33*, L19105, doi:10.1029/2006GL027243.
Anderson, B. J., K. Takahashi, and B. A. Toth (2000), Sensing global Birkeland currents with Iridium® engineering magnetometer data, *Geophys. Res. Lett.*, *27*(24), 4045–4048.
Angelopoulos, V. (2009), *The THEMIS Mission*, Springer, New York.
Angelopoulos, V., et al. (2008), Tail reconnection triggering substorm onset, *Science*, *321*(5891), 931–935.
Angelopoulos, V., et al. (2009), First results from the THEMIS mission, in *The THEMIS Mission*, pp. 453–476, Springer, New York.
Auster, H., et al. (2009), The THEMIS fluxgate magnetometer, in *The THEMIS Mission*, pp. 235–264, Springer, New York.
Baker, D., T. Fritz, R. McPherron, D. Fairfield, Y. Kamide, and W. Baumjohann (1985), Magnetotail energy storage and release during the CDAW 6 substorm analysis intervals, *J. Geophys. Res.*, *90*, 1205–1216.
Baker, D. N., T. Pulkkinen, V. Angelopoulos, W. Baumjohann, and R. McPherron (1996), Neutral line model of substorms: Past results and present view, *J Geophys. Res.*, *101*, 12–975.
Baumjohann, W., G. Paschmann, and C. Cattell (1989), Average plasma properties in the central plasma sheet, *J. Geophys. Res.*, *94*(A6), 6597–6606.
Birn, J., and M. Hesse (2013), The substorm current wedge in MHD simulations, *J. Geophys. Res. Space Physics*, *118*, 3364–3376, doi:10.1002/jgra.50187.
Birn, J., M. Hesse, G. Haerendel, W. Baumjohann, and K. Shiokawa (1999), Flow braking and the substorm current wedge, *J. Geophys. Res.*, *104*(A9), 19,895–19,903.
Birn, J., A. Artemyev, D. Baker, M. Echim, M. Hoshino, and L. Zelenyi (2012), Particle acceleration in the magnetotail and aurora, *Space Sci. Rev.*, *173*(1–4), 49–102.
Birn, J., M. Hesse, R. Nakamura, and S. Zaharia (2013), Particle acceleration in dipolarization events, *J. Geophys. Res. Space Physics*, *118*, 1960–1971, doi:10.1002/jgra.50132.
Boström, R. (1964), A model of the auroral electrojets, *J. Geophys. Res.*, *69*(23), 4983–4999.
Cao, J.-B., et al. (2010), Geomagnetic signatures of current wedge produced by fast flows in a plasma sheet, *J. Geophys. Res.*, *115*, A08205, doi:10.1029/2009JA014891.
Chaston, C., et al. (2010), Motion of aurorae, *Geophys. Res. Lett.*, *37*, L08104, doi:10.1029/2009GL042117.
Craven, J. D., and L. A. Frank (1987), Latitudinal motions of the aurora during substorms, *J. Geophys. Res.*, *92*(A5), 4565–4573.
Du, J., T. Zhang, R. Nakamura, C. Wang, W. Baumjohann, A. Du, M. Volwerk, K.-H. Glassmeier, and J. McFadden (2011), Mode conversion between Alfvén and slow waves observed in the magnetotail by THEMIS, *Geophys. Res. Lett.*, *38*, L07101, doi:10.1029/2011GL046989.
Duan, S., et al. (2011), Multiple magnetic dipolarizations observed by THEMIS during a substorm, *Ann. Geophys.*, *29*, 331–339.
Dungey, J. W. (1961), Interplanetary magnetic field and the auroral zones, *Phys. Rev. Lett.*, *6*(2), 47–48.
Elphinstone, R., et al. (1995), The double oval UV auroral distribution: 1. Implications for the mapping of auroral arcs, *J. Geophys. Res.*, *100*(A7), 12,075–12,092.
Forsyth, C., M. Lester, R. Fear, E. Lucek, I. Dandouras, A. Fazakerley, H. Singer, and T. K. Yeoman (2009), Solar wind and substorm excitation of the wavy current sheet, *Ann. Geophys.*, *27*, 2457–2474.
Fu, H. S., Y. V. Khotyaintsev, M. André, and A. Vaivads (2011), Fermi and betatron acceleration of suprathermal electrons behind dipolarization fronts, *Geophys. Res. Lett.*, *38*, L16104, doi:10.1029/2011GL048528.
Hasegawa, A. (1976), Particle acceleration by MHD surface wave and formation of aurora, *J. Geophys. Res.*, *81*(28), 5083–5090.
Henderson, M. G. (2009), Observational evidence for an inside-out substorm onset scenario, *Ann. Geophys.*, *27*, 2129–2140.
Hones, E. (1977), Substorm processes in the magnetotail: Comments on "On hot tenuous plasmas, fireballs, and boundary layers in the Earth's magnetotail" by La Frank, KL ackerson, and RP lepping, *J. Geophys. Res.*, *82*(35), 5633–5640.

Hsu, T.-S., and R. L. McPherron (2003), Occurrence frequencies of IMF triggered and nontriggered substorms, *J. Geophys. Res.*, *108*(A7), 1307, doi:10.1029/2002JA009442.
Jacquey, C., J. Sauvaud, J. Dandouras, and A. Korth (1993), Tailward propagating cross-tail current disruption and dynamics of near-Earth tail: A multi-point measurement analysis, *Geophys. Res. Lett.*, *20*(10), 983–986.
Kalmoni, N. M., I. J. Rae, C. E. Watt, K. R. Murphy, C. Forsyth, and C. J. Owen (2015), Statistical characterization of the growth and spatial scales of the substorm onset arc, *J. Geophys. Res. Space Physics*, *120*, 8503–8516, doi:10.1002/2015JA021470.
Keiling, A., et al. (2008), Multiple intensifications inside the auroral bulge and their association with plasma sheet activities, *J. Geophys. Res.*, *113*, 8503–8516, doi:10.1002/2015JA021470.
Keiling, A., et al. (2009), Substorm current wedge driven by plasma flow vortices: THEMIS observations, *J. Geophys. Res.*, *114*, A00C22, doi:10.1029/2009JA014114.
Kepko, L., M. Kivelson, and K. Yumoto (2001), Flow bursts, braking, and Pi2 pulsations, *J. Geophys. Res.*, *106*(A2), 1903–1915.
Liang, J., E. Donovan, W. Liu, B. Jackel, M. Syrjäsuo, S. Mende, H. Frey, V. Angelopoulos, and M. Connors (2008), Intensification of preexisting auroral arc at substorm expansion phase onset: Wave-like disruption during the first tens of seconds, *Geophys. Res. Lett.*, *35*, L17S19, doi:10.1029/2008GL033666.
Liou, K., C.-I. Meng, P. Newell, A. Lui, G. Reeves, and R. Belian (2001), Particle injections with auroral expansions, *J. Geophys. Res.*, *106*(A4), 5873–5881.
Lui, A. (1991), A synthesis of magnetospheric substorm models, *J. Geophys. Res.*, *96*(A2), 1849–1856.
Lui, A. (1996), Current disruption in the Earth's magnetosphere: Observations and models, *J. Geophys. Res.*, *101*(A6), 13,067–13,088.
Lui, A. (2004), Potential plasma instabilities for substorm expansion onsets, *Space Sci. Rev.*, *113*(1–2), 127–206.
Lui, A. (2009), Comment on tail reconnection triggering substorm onset, *Science*, *324*(5933), 1391–1391.
Lui, A. (2011), Reduction of the cross-tail current during near-Earth dipolarization with multisatellite observations, *J. Geophys. Res.*, *116*, A12239, doi:10.1029/2011JA017107.
Lui, A. (2013), Cross-tail current evolution during substorm dipolarization, *Ann. Geophys.*, *31*, 1131–1142.
Lui, A. (2015), Dipolarization fronts and magnetic flux transport, *Geosci. Lett.*, *2*(1), 1–8.
Lui, A., et al. (2008), Determination of the substorm initiation region from a major conjunction interval of THEMIS satellites, *J. Geophys. Res.*, *113*, A00C04, doi:10.1029/2008JA013424.
Lui, A., E. Spanswick, E. Donovan, J. Liang, W. Liu, O. LeContel, and Q.-G. Zong (2010), A transient narrow poleward extrusion from the diffuse aurora and the concurrent magnetotail activity, *J. Geophys. Res.*, *115*, A10210, doi:10.1029/2010JA015449.
Marklund, G. T., S. Sadeghi, T. Karlsson, P.-A. Lindqvist, H. Nilsson, C. Forsyth, A. Fazakerley, E. A. Lucek, and J. Pickett (2011), Altitude distribution of the auroral acceleration potential determined from Cluster satellite data at different heights, *Phys. Rev. Lett.*, *106*(5), 055002.
McFadden, J., C. Carlson, D. Larson, M. Ludlam, R. Abiad, B. Elliott, P. Turin, M. Marckwordt, and V. Angelopoulos (2008), The THEMIS ESA plasma instrument and in-flight calibration, *Space Sci. Rev.*, *141*(1–4), 277–302.
McPherron, R., C. Russell, M. Kivelson, and P. Coleman (1973), Substorms in space: The correlation between ground and satellite observations of the magnetic field, *Radio Sci.*, *8*(11), 1059–1076.
Mende, S., S. Harris, H. Frey, V. Angelopoulos, C. Russell, E. Donovan, B. Jackel, M. Greffen, and L. Peticolas (2009), The THEMIS array of ground-based observatories for the study of auroral substorms, in *The THEMIS Mission*, pp. 357–387, Springer, New York.
Mende, S. B., H. U. Frey, C. W. Carlson, J. McFadden, J.-C. Gérard, B. Hubert, S. A. Fuselier, G. Gladstone, and J. L. Burch (2002), IMAGE and FAST observations of substorm recovery phase aurora, *Geophys. Res. Lett.*, *29*(12), 43–1 – 43-4, doi:10.1029/2001GL013027.
Murphy, K. R., I. R. Mann, I. J. Rae, C. L. Waters, B. J. Anderson, D. K. Milling, H. J. Singer, and H. Korth (2012), Reduction in field-aligned currents preceding and local to auroral substorm onset, *Geophys. Res. Lett.*, *39*, L15106, doi:10.1029/2012GL052798.
Murphy, K. R., I. R. Mann, I. J. Rae, A. P. Walsh, and H. U. Frey (2014), Inner magnetospheric onset preceding reconnection and tail dynamics during substorms: Can substorms initiate in two different regions?, *J. Geophys. Res. Space Physics*, *119*, 9684–9701, doi:10.1002/2014JA019795.
Nagai, T., D. Baker, and P. Higbie (1983), Development of substorm activity in multiple-onset substorms at synchronous orbit, *J. Geophys. Res.*, *88*(A9), 6994–7004.
Nakamizo, A., and T. Iijima (2003), A new perspective on magnetotail disturbances in terms of inherent diamagnetic processes, *J. Geophys. Res.*, *108*, 1286, doi:10.1029/2002JA009400.
Nakamura, R., W. Baumjohann, R. Schödel, M. Brittnacher, V. Sergeev, M. Kubyshkina, T. Mukai, and K. Liou (2001), Earthward flow bursts, auroral streamers, and small expansions, *J. Geophys. Res.*, *106*(A6), 10,791–10,802.
Nakamura, R., et al. (2006), Dynamics of thin current sheets associated with magnetotail reconnection, *J. Geophys. Res.*, *111*, A11206, doi:10.1029/2006JA011706.
Nishimura, Y., L. Lyons, T. Kikuchi, V. Angelopoulos, E. Donovan, S. Mende, P. Chi, and T. Nagatsuma (2012), Formation of substorm Pi2: A coherent response to auroral streamers and currents, *J. Geophys. Res.*, *117*, A09218, doi:10.1029/2012JA017889.
Ohtani, S., R. Yamaguchi, H. Kawano, F. Creutzberg, J. Sigwarth, L. Frank, and T. Mukai (2002), Does the braking of the fast plasma flow trigger a substorm?: A study of the August 14, 1996, event, *Geophys. Res. Lett.*, *29*(15), 1721, doi:10.1029/2001GL013785.
Ohtani, S.-I (2004), Flow bursts in the plasma sheet and auroral substorm onset: Observational constraints on connection between midtail and near-Earth substorm processes, *Space Sci. Rev.*, *113*(1–2), 77–96.
Palin, L., et al. (2015), Three-dimensional current systems and ionospheric effects associated with small dipolarization fronts, *J. Geophys. Res. Space Physics*, *120*, 3739–3757, doi:10.1002/2015JA021040.
Parks, G. K. (1991), *Physics of Space Plasmas: An Introduction*, Addison-Wesley Publ. Co., Redwood City, Calif.
Partamies, N., O. Amm, K. Kauristie, T. Pulkkinen, and E. Tanskanen (2003), A pseudo-breakup observation: Localized current wedge across the postmidnight auroral oval, *J. Geophys. Res.*, *108*(A1), 1020, doi:10.1029/2002JA009276.
Pu, Z., et al. (1997), MHD drift ballooning instability near the inner edge of the near-Earth plasma sheet and its application to substorm onset, *J. Geophys. Res.*, *102*(A7), 14,397–14,406.
Pu, Z., et al. (2010), THEMIS observations of substorms on 26 February 2008 initiated by magnetotail reconnection, *J. Geophys. Res.*, *115*, A02212, doi:10.1029/2009JA014217.
Pulkkinen, T., D. Baker, M. Wiltberger, C. Goodrich, R. Lopez, and J. Lyon (1998), Pseudobreakup and substorm onset: Observations and MHD simulations compared, *J. Geophys. Res.*, *103*(A7), 14,847–14,854.
Pytte, T., R. McPherron, and S. Kokubun (1976), The ground signatures of the expansion phase during multiple onset substorms, *Planet. Space Sci.*, *24*(12), 1115–1132.
Rae, I. J., et al. (2009), Near-Earth initiation of a terrestrial substorm, *J. Geophys. Res.*, *114*, A07220, doi:10.1029/2008JA013771.
Rostoker, G. (1998), On the place of the pseudo-breakup in a magnetospheric substorm, *Geophys. Res. Lett.*, *25*(2), 217–220.

Rostoker, G., S. Akasofu, J. Foster, R. Greenwald, A. Lui, Y. Kamide, K. Kawasaki, R. McPherron, and C. Russell (1980), Magnetospheric substorms—Definition and signatures, *J. Geophys. Res.*, *85*, 1663–1668.
Runov, A., et al. (2005), Electric current and magnetic field geometry in flapping magnetotail current sheets, *Ann. Geophys.*, *23*, 1391–1403.
Saito, M., Y. Miyashita, M. Fujimoto, K. Liou, Y. Saito, and J. Sigwarth (2010), Stepwise feature of aurora during substorm expansion compared with the near-Earth tail dipolarization: Possible types of substorm dynamics, *J. Geophys. Res.*, *115*, A02207, doi:10.1029/2009JA014572.
Sergeev, V., et al. (2003), Current sheet flapping motion and structure observed by Cluster, *Geophys. Res. Lett.*, *30*(6), 1327, doi:10.1029/2002GL016500.
Sergeev, V., V. Angelopoulos, M. Kubyshkina, E. Donovan, X.-Z. Zhou, A. Runov, H. Singer, J. McFadden, and R. Nakamura (2011), Substorm growth and expansion onset as observed with ideal ground-spacecraft THEMIS coverage, *J. Geophys. Res.*, *116*, A00I26, doi:10.1029/2010JA015689.
Sharber, J., and W. Heikkila (1972), Fermi acceleration of auroral particles, *J. Geophys. Res.*, *77*(19), 3397–3410.
Shiokawa, K., W. Baumjohann, and G. Haerendel (1997), Braking of high-speed flows in the near-Earth tail, *Geophys. Res. Lett.*, *24*(10), 1179–1182.
Southwood, D., and M. Saunders (1985), Curvature coupling of slow and Alfvén MHD waves in a magnetotail field configuration, *Planet. Space Sci.*, *33*(1), 127–134.
Tang, C., L. Lu, M. Zhou, and Z. Yao (2013), THEMIS observations of electron acceleration associated with the evolution of substorm dipolarization in the near-Earth tail, *J. Geophys. Res. Space Physics*, *118*, 4237–4247, doi:10.1002/jgra.50418.
Tsyganenko, N., and M. Sitnov (2005), Modeling the dynamics of the inner magnetosphere during strong geomagnetic storms, *J. Geophys. Res.*, *110*, A03208, doi:10.1029/2004JA010798.
Volwerk, M., et al. (2003), A statistical study of compressional waves in the tail current sheet, *J. Geophys. Res.*, *108*(A12), 1429, doi:10.1029/2003JA010155.
Walsh, A., C. Owen, A. Fazakerley, C. Forsyth, and I. Dandouras (2011), Average magnetotail electron and proton pitch angle distributions from Cluster PEACE and CIS observations, *Geophys. Res. Lett.*, *38*, L06103, doi:10.1029/2011GL046770.
Waters, C., B. Anderson, and K. Liou (2001), Estimation of global field aligned currents using the Iridium system magnetometer data, *Geophys. Res. Lett*, *28*(11), 2165–2168.
Wu, P., T. Fritz, B. Larvaud, and E. Lucek (2006), Substorm associated magnetotail energetic electrons pitch angle evolutions and flow reversals: Cluster observation, *Geophys. Res. Lett.*, *33*, L17101, doi:10.1029/2006GL026595.
Xing, X., C.-P. Wang, J. Liang, and L. R. Lyons (2015), Plasma sheet Pi2 pulsations associated with bursty bulk flows, *J. Geophys. Res. Space Physics*, *120*, 8692–8706, doi:10.1002/2015JA021668.
Yao, Z., et al. (2012), Mechanism of substorm current wedge formation: THEMIS observations, *Geophys. Res. Lett.*, *39*, L13102, doi:10.1029/2012GL052055.
Yao, Z., et al. (2013), Conjugate observations of flow diversion in the magnetotail and auroral arc extension in the ionosphere, *J. Geophys. Res. Space Physics*, *118*, 4811–4816, doi:10.1002/jgra.50419.
Yao, Z., et al. (2014), Current reduction in a pseudo-breakup event: THEMIS observations, *J. Geophys. Res. Space Physics*, *119*(10), 8178–8187, doi:10.1002/2014JA020186.
Yao, Z., et al. (2015), A physical explanation for the magnetic decrease ahead of dipolarization fronts, *Ann. Geophys.*, *33*, 1301–1309.